Temperature sensor based on a hybrid ITO-silica resonant cavity

Abian B. Socorro,[1,4] Soheil Soltani,[2,7] Ignacio Del Villar,[1,5] Jesus M. Corres,[1,6] and Andrea M. Armani[2,3,*]

[1]*Electric and Electronic Engineering Department, Public University of Navarra, 31006 Pamplona, Spain.*
[2]*Ming Hsieh Department of Electrical Engineering-Electrophysics, University of Southern California, Los Angeles, California 90089, USA*
[3]*Mork Family Department of Chemical Engineering and Materials Science, University of Southern California, Los Angeles, California 90089, USA*
[4]*ab.socorro@unavarra.es*
[5]*ignacio.delvillar@unavarra.es*
[6]*jmcorres@unavarra.es*
[7]*soheilso@usc.edu,*
**armani@usc.edu*

Abstract: Integrated optical devices comprised of multiple material systems are able to achieve unique performance characteristics, enabling applications in sensing and in telecommunications. Due to ease of fabrication, the majority of previous work has focused on polymer-dielectric or polymer-semiconductor systems. However, the environmental stability of polymers is limited. In the present work, a hybrid device comprised of an indium tin oxide (ITO) coating on a silicon dioxide toroidal resonant cavity is fabricated. Finite element method simulations of the optical field in the multi-material device are performed, and the optical mode profile is significantly altered by the high index film. The quality factor is also measured and is material loss limited. Additionally, its performance as a temperature sensor is characterized. Due to the high thermo-optic coefficient of ITO and the localization of the optical field in the ITO layer, the hybrid temperature sensor demonstrates a nearly 3-fold improvement in performance over the conventional silica device.

OCIS codes: (230.5750) Resonators; (130.3120) Integrated optics devices; (160.6840) Thermo-optical materials; (160.6060) Solgel.

References and links

1. C. J. Barrelet, J. M. Bao, M. Loncar, H. G. Park, F. Capasso, and C. M. Lieber, "Hybrid single-nanowire photonic crystal and microresonator structures," Nano Lett. **6**(1), 11–15 (2006).
2. L. Chen and R. M. Reano, "Compact electric field sensors based on indirect bonding of lithium niobate to silicon microrings," Opt. Express **20**(4), 4032–4038 (2012).
3. D. X. Dai and S. L. He, "A silicon-based hybrid plasmonic waveguide with a metal cap for a nano-scale light confinement," Opt. Express **17**(19), 16646–16653 (2009).
4. B. Guha, K. Preston, and M. Lipson, "Athermal silicon microring electro-optic modulator," Opt. Lett. **37**(12), 2253–2255 (2012).
5. C. Y. Jeong and S. Kim, "Dominant mode control of a graphene-embedded hybrid plasmonic resonator for a tunable nanolaser," Opt. Express **22**(12), 14819–14829 (2014).
6. C. Shi, S. Soltani, and A. M. Armani, "Gold nanorod plasmonic upconversion microlaser," Nano Lett. **13**(12), 5827–5831 (2013).
7. S. Mehrabani, P. Kwong, M. Gupta, and A. M. Armani, "Hybrid microcavity humidity sensor," Appl. Phys. Lett. **102**(24), 241101 (2013).
8. S. Mehrabani, A. J. Maker, and A. M. Armani, "Hybrid Integrated Label-Free Chemical and Biological Sensors," Sensors (Basel) **14**(4), 5890–5928 (2014).
9. M. A. Schmidt, D. Y. Lei, L. Wondraczek, V. Nazabal, and S. A. Maier, "Hybrid nanoparticle-microcavity-based plasmonic nanosensors with improved detection resolution and extended remote-sensing ability," Nat Commun **3**, 1108 (2012).
10. M. A. Santiago-Cordoba, S. V. Boriskina, F. Vollmer, and M. C. Demirel, "Nanoparticle-based protein detection by optical shift of a resonant microcavity," Appl. Phys. Lett. **99**(7), 073701 (2011).

#224193 - $15.00 USD Received 1 Oct 2014; revised 20 Nov 2014; accepted 25 Nov 2014; published 26 Jan 2015

11. H. Wang, L. Zhu, and W. Menzel, "Ultra-wideband bandpass filter with hybrid microstrip/CPW structure," IEEE Microw. Wirel. Compon. Lett. **15**(12), 844–846 (2005).
12. H.-S. Choi and A. M. Armani, "Thermal non-linear effects in hybrid optical microresonators," Appl. Phys. Lett. **97**(22), 223306 (2010).
13. C. R. Z. I. Del Villar, P. Sánchez, M. Hernáez, C. F. Valdivielso, F. J. Arregui, and I. R. Matías, "Generation of lossy mode resonances by deposition of high-refractive-index coatings on uncladded multimode optical fibers," J. Opt. **12**(9), 095503 (2010).
14. H. S. Choi, S. Ismail, and A. M. Armani, "Studying polymer thin films with hybrid optical microcavities," Opt. Lett. **36**(11), 2152–2154 (2011).
15. A. B. Matsko and V. S. Ilchenko, "Optical Resonators with Whispering-Gallery Modes-Part I: Basics," IEEE J. Sel. Top. Quantum Electron. **12**(1), 3–14 (2006).
16. H.-S. Choi, X. Zhang, and A. M. Armani, "Hybrid Silica-Polymer Ultra-High-Q Microresonators," Opt. Lett. **35**(4), 459–461 (2010).
17. B. A. Rose, A. J. Maker, and A. M. Armani, "Characterization of thermo-optic coefficient and material loss of high refractive index silica sol-gel films in the visible and near-IR," Opt. Mater. Express **2**(5), 671–681 (2012).
18. H. K. Hunt and A. M. Armani, "Label-Free Biological and Chemical Sensors," Nanoscale **2**(9), 1544–1559 (2010).
19. M. S. Luchansky and R. C. Bailey, "High-Q Optical Sensors for Chemical and Biological Analysis," Anal. Chem. **84**(2), 793–821 (2012).
20. M. I. Cheema, S. Mehrabani, A. A. Hayat, Y. A. Peter, A. M. Armani, and A. G. Kirk, "Simultaneous measurement of quality factor and wavelength shift by phase shift microcavity ring down spectroscopy," Opt. Express **20**(8), 9090–9098 (2012).
21. Y. Lin, V. Ilchenko, J. Nadeau, and L. Maleki, "Biochemical detection with optical whispering-gallery resonators," in *Laser Resonators and Beam Control IX*, (SPIE, 2007), U4520–U4520.
22. J. Knittel, J. D. Swaim, D. L. McAuslan, G. A. Brawley, and W. P. Bowen, "Back-scatter based whispering gallery mode sensing," Sci Rep **3**, 2974 (2013).
23. D. K. Armani, T. J. Kippenberg, S. M. Spillane, and K. J. Vahala, "Ultra-high-Q toroid microcavity on a chip," Nature **421**(6926), 925–928 (2003).
24. M. Cai, O. Painter, and K. J. Vahala, "Observation of critical coupling in a fiber taper to a silica-microsphere whispering-gallery mode system," Phys. Rev. Lett. **85**(1), 74–77 (2000).
25. A. Yariv, "Universal relations for coupling of optical power between microresonators and dielectric waveguides," Electron. Lett. **36**(4), 321–333 (2000).
26. S. Soltani and A. M. Armani, "Optothermal transport behavior in whispering gallery mode optical cavities," Appl. Phys. Lett. **105**(5), 051111 (2014).
27. H.-S. Choi and A. M. Armani, "Thermal non-linear effects in hybrid optical microresonators," Appl. Phys. Lett. **97**(22), 223306 (2010).
28. S. Wiechmann and J. Müller, "Thermo-optic properties of TiO_2, Ta_2O_5 and Al_2O_3 thin films for integrated optics on silicon," Thin Solid Films **517**(24), 6847–6849 (2009).

1. Introduction

In recent years, extensive research efforts have focused on developing new optical materials to enhance the performance of integrated optical devices for a wide range of applications including optical switches, lasers and sensors [1–11]. One reason for the broad impact is the numerous possible combinations of functional materials and optical devices. For example, hybrid devices have demonstrated athermal behavior and ultra-low threshold lasing [4–6,12]. While initial research focused on telecommunications applications, more recently, the research has shifted its emphasis to detection applications; specifically, using materials to manipulate the optical field profile while adding functionality to the device [7–9].

While there are many types of optical sensors, one common element is that the strength of the signal is related to the intensity of the optical field. The conventional approach to increase the optical field intensity is to increase in the input power. However, an alternative approach is to modify the optical field distribution in the sensor. One method for compressing the field and increasing the sensitivity limit is to create a hybrid device, comprised of multiple materials. In this pursuit, a wide range of new materials has been developed. For example, metal nanoparticles have been used in combination with a wide range of devices for field enhancement [9, 10]. While very successful, metal nanoparticles are also extremely lossy. Therefore, the total number of nanoparticles that can be used in a single device is limited.

An alternate approach is to use a low-loss material, such as a high index oxide, to improve the optical field confinement in the sensing area and to increase the sensing signal. While several high index oxides have been developed, research thus far has focused on waveguide devices [13]. By combining these materials with higher performance devices, the benefit to

#224193 - $15.00 USD Received 1 Oct 2014; revised 20 Nov 2014; accepted 25 Nov 2014; published 26 Jan 2015

the overall sensing system will be greater. In previous work, a hybrid sensor system comprised of polymer coated resonant cavities was demonstrated for temperature detection [14]. However, polymer-based systems face numerous limitations, particularly in the field of temperature detection, where the glass transition temperature of the polymer will limit the ultimate working range of the device.

In the present work, we coat a Silica high quality factor (Q) microcavity with Indium Tin Oxide (ITO) and demonstrate thermal sensing. Using this hybrid device in combination with finite element model simulations, we experimentally measure the thermo-optic coefficient of ITO, which is approximately 18 times larger than silica. Because of the significant increase refractive index as compared to silica, the optical mode profile changes. In temperature sensing experiments, the combination of optical field change and dn/dT increase results in a 2-3-fold increase in temperature response.

2. Theory

2.1 Quality factor limits in hybrid cavities

In a whispering gallery mode optical cavity, the quality factor is comprised of extrinsic and intrinsic losses [15]. While the extrinsic losses are primarily determined by the coupling method used, the intrinsic losses are inherent to the cavity. In hybrid cavities or thin film coated cavities, previous work has shown that the quality factor is limited by the material loss of the system [16,17]. This loss can be analytically described by (1)

$$Q_{mat} = \frac{2\pi n_{eff}}{\lambda \alpha_{eff}} \tag{1}$$

where n_{eff} is the effective refractive index, λ is the resonant wavelength and α_{eff} is the effective material loss. The expressions for n_{eff} and α_{eff} are approximately given by (2) and (3):

$$n_{eff} = \beta \cdot n_{cavity} + \gamma \cdot n_{film} + \delta \cdot n_{air} \tag{2}$$

$$\alpha_{eff} = \beta \cdot \alpha_{cavity} + \gamma \cdot \alpha_{film} + \delta \cdot \alpha_{air} \tag{3}$$

respectively, where β, γ, and δ are the portion of the optical field located in the cavity, film and air. For toroidal optical resonant cavities, which are the focus of the present work, these values are determined using finite element method simulations, and $\beta + \gamma + \delta = 1$.

2.2 Thermo-optic coefficient (dn/dT)

The thermo-optic effect describes the temperature-dependent refractive index change of a material. In dielectric materials, the thermo-optic coefficient (dn/dT) is typically positive, resulting in an increase in refractive index as the temperature increases. In hybrid cavities, by derivating expression (2) with respect of the temperature, we obtain expression (4), which describes this variation [17]:

$$\frac{dn_{eff}}{dT} = \beta \cdot \frac{dn_{cavity}}{dT} + \gamma \cdot \frac{dn_{film}}{dT} + \delta \cdot \frac{dn_{air}}{dT} \tag{4}$$

Again, the coefficients β, γ and δ are the portion of the optical field ($|E|^2$) located in the cavity, film and air and they are determined using finite element method modeling. Given that dn/dT of silica and air are known, from the experimental data and the FEM model, it is possible to determine the dn/dT of the film.

2.3 Temperature detection

Resonant cavity-based detection relies on the dependence of the resonant wavelength on the cavity's refractive index and geometrical parameters [18, 19]. Previous work has

#224193 - $15.00 USD Received 1 Oct 2014; revised 20 Nov 2014; accepted 25 Nov 2014; published 26 Jan 2015

demonstrated cavity-based sensing using a variety of mechanisms (e.g. phase, transmission, optical loss, resonant wavelength); however, the resonant wavelength change approach is the most commonly used [7, 8, 10, 20–22].

In the case of thermal sensing, the thermo-optic effect is particularly important. Assuming that thermo-optic effect is the dominant mechanism, the resonant wavelength is directly related to the refractive index of the cavity according the relationship:

$$\frac{\Delta\lambda}{\Delta T} = \frac{dn_{eff}}{dT} \cdot \frac{\lambda}{n_{eff}} \tag{5}$$

where Δλ is the change in resonant wavelength and ΔT is the change in temperature [14]. Therefore, by increasing the thermo-optic coefficient, the sensor will generate a larger signal, improving the overall sensor performance.

2.4 FEM modeling

To determine the optical field distribution in the different regions of the hybrid device, finite element method (FEM) simulations are performed using COMSOL Multiphysics [16]. The modeling parameters are determined by the experimental conditions to allow direct comparison between the results. The toroid major and minor diameters are 60 microns and 7 microns, and the wavelength is 780 nm. The refractive index and film thickness of the ITO is measured using ellipsometry. All other constants used in the simulations are taken from the COMSOL library. In order to improve the simulation efficiency, the mesh size was chosen to be 1/10th of the wavelength inside the structure. By controlling the azimuthal mode order (M) in the cavity, we can determine the optical field distribution, which corresponds to the values for β, γ, and δ.

A pair of simulations is shown in Figs. 1(a) and 1(b). In the first simulation, the film has the same properties as the silica toroid; as a result, the film simply increases the diameter of the device and the optical field is not perturbed or changed by the presence of the film. In contrast, in the second simulation, an ITO film is used. By comparing these two simulations, it becomes evident that several significant changes occur.

First, due to the large refractive index contrast between the coating and the resonator, the mode is split when the ITO film is included. While the majority of the optical mode pushed back into the resonator, a small optical lobe appears inside the coating. This effect is apparent in Fig. 1(c). This small, secondary field lobe changes how the optical field interacts with the coating.

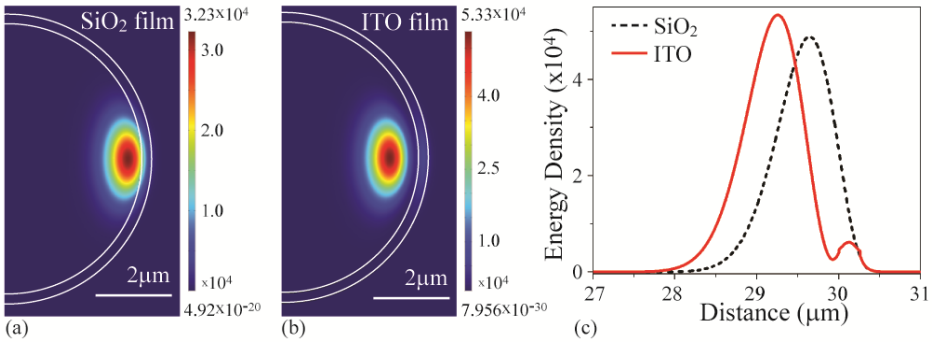

Fig. 1. FEM modeling results. In both models, the films are 260nm thick. Optical field distribution with a) an SiO_2 film and b) an ITO film. c) Modal energy density distribution cross section in the device with both films. The periphery of the device or silica-film interface occurs at 30μm. The optical field clearly changes both shape and distribution with the high index film.

#224193 - $15.00 USD Received 1 Oct 2014; revised 20 Nov 2014; accepted 25 Nov 2014; published 26 Jan 2015

3. Device fabrication and characterization

3.1 Material synthesis and characterization

To make the ITO coating, first, an ITO sol-gel solution is made. The stock solution is synthesized by combining 30 ml ethanol (CH_2OH), 35 mg tin chloride ($SnCl_4$) and 200 mg indium chloride ($InCl_3$), and stirring them for 3 hours. Then, 1 ml of Tween 80® is added, obtaining the sol-gel solution after 2 additional hours of stirring. Throughout the process, the solution is kept at 25°C, and it is vortexed several times, to minimize the formation of aggregates.

After preparing the wafer surface using an oxygen plasma to increase the hydrophilicity, the ITO is deposited twice on the SiO_2/Si wafer using spin-coating to form a uniform thin film. The first ITO layer is deposited by dropping the solution on the samples and spin-coating at 7000 rpm for 30 seconds. The samples are annealed at 500°C for 20 minutes in an ambient environment. The samples are immediately removed from the furnace after 20 minutes. A second ITO layer is deposited using the same process. However, the annealing methods are changed. This time, after 20 minutes, the samples remain in the furnace as the temperature is incrementally decreased from 500°C to room temperature at a rate of 1°C/min. This gradual decrease allows very smooth, defect-free films to be produced.

The thickness and refractive index of the ITO and SiO_2 films are measured using spectroscopic ellipsometry at 780nm. The ITO film is 260 nm thick, and the index values are 1.45367 and 1.7871 for SiO_2 and ITO, respectively. These values are used to determine the n_{eff} and dn_{eff}/dT in subsequent calculations.

3.2 Device fabrication

The hybrid ITO-silica toroidal cavity fabrication process has two distinct steps: 1) fabricate the silica toroidal cavities, and 2) conformally coat the cavities with the ITO thin film.

The silica toroidal cavities are fabricated in three steps on silicon wafers with two microns of thermally grown oxide [23]. First, 80-micron diameter circular pads are defined using photolithography and buffered oxide etching. Then, the silica microdisks are created by undercutting the oxide with xenon difluoride. Finally, the silica toroidal cavity is made by reflowing the silica microdisk with a carbon dioxide laser. The ITO films are deposited and annealed using the same method described previously. The deposition of the ITO is verified using electron diffraction spectroscopy (EDS) in combination with an SEM/FIB system. Based on the EDS, the ITO film conformally coats the toroidal structure (top, side and underneath). As can be observed in Fig. 2(a), the ITO coating is quite uniform and defect-free.

3.3 Device characterization

To measure the quality factor, the device is coupled to a narrow linewidth tunable laser centered at 765nm (Velocity, Newport) using a tapered optical fiber waveguide. Tapered optical fiber waveguides are a low loss, high efficiency evanescent coupling method [24]. As such, the coupling losses are minimal, allowing the intrinsic Q of the cavity to be determined [25]. The waveguide is aligned with the cavity, using top and side view cameras and a 3-axis nano-positioning stage. The output from the waveguide is sent to a photodetector, and the signal is monitored on an integrated digitizer/oscilloscope. By scanning across a series of wavelengths, a resonant wavelength (λ) can be identified and recorded. The spectrum is fit to a Lorentzian, and the cavity Q is determined according to: $Q = \lambda/\Delta\lambda$, where $\Delta\lambda$ is the linewidth. The scan range, scan frequency and input power are optimized to minimize any thermal distortion of the resonant linewidth [12].

#224193 - $15.00 USD Received 1 Oct 2014; revised 20 Nov 2014; accepted 25 Nov 2014; published 26 Jan 2015

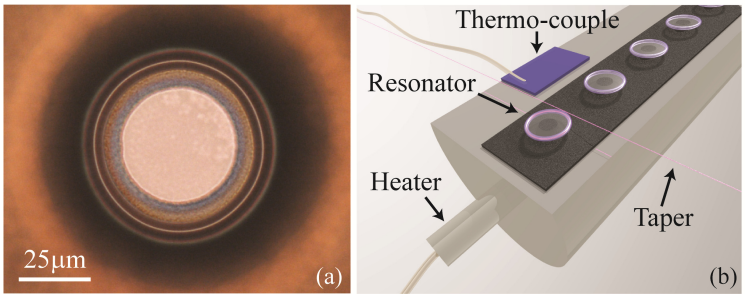

Fig. 2. a) An optical micrograph of an ITO-coated silica toroidal cavity. b) A schematic of the testing set-up, with the key components of the temperature control stage and the relative positions of the taper and the resonant cavity indicated.

3.4 Sensing measurements

To characterize the thermal response of the device, a temperature control stage with a thermo-couple controlled feedback loop is integrated into the previously described set-up (Fig. 2 (b)) [12]. Using this stage, the device can be heated in 0.5°C steps with minimal overshoot. Two different, complementary approaches are used to measure the temperature response of the ITO-SiO_2 hybrid cavity. Additionally, for comparison, the response of a plain SiO_2 cavity was also measured.

In the first method, the minimum position (wavelength) and the transmission (coupled power) are continuously tracked and recorded at a frequency of 691 pts/min. This approach has several advantages. Because the transmission point is recorded, we can detect changes in coupling, also known as "taper jitter". This jitter is widely acknowledged to be a source of noise in high Q cavity measurements. Therefore, using this method, we are now able to isolate and remove these points with automated filters without comprising the volume of results (e.g. reject all data with transmission variation >5%). Additionally, we can perform statistically significant error analysis on the wavelength change. However, the high-speed acquisition is only possible because the whole spectra is not recorded; thus, we lose information about the cavity Q.

In the second method, resonance spectra are recorded at the distinct temperature points. Specifically, after changing the temperature, the resonance is allowed to stabilize, and then the spectra is saved. Based on a Lorentzian fit, the resonant wavelength and the loaded Q are determined. However, because of the amount of time it takes to save an entire spectrum, it is not possible to use this approach to perform real-time detection; for similar reasons, acquiring a sufficiently large amount of data for statistical analysis is unrealistic. It is important to note that during the measurements, the coupling is not changed. Therefore, even small changes in the extrinsic loss (or coupling loss) will be detected.

4. Results and analysis

4.1 Quality factor

As mentioned, there are many factors that can contribute to the degradation of the cavity Q, most notably surface scattering and material loss. In sol-gel coated hybrid cavities, it is critical to optimize the annealing of the sol-gel film, as small cracks in the film will give rise to large scattering losses. As can be observed in Fig. 3, in the present ITO-SiO_2 hybrid cavities, loaded Q factors above $1x10^5$ are obtained. These values indicate that the Q is material limited.

#224193 - $15.00 USD Received 1 Oct 2014; revised 20 Nov 2014; accepted 25 Nov 2014; published 26 Jan 2015

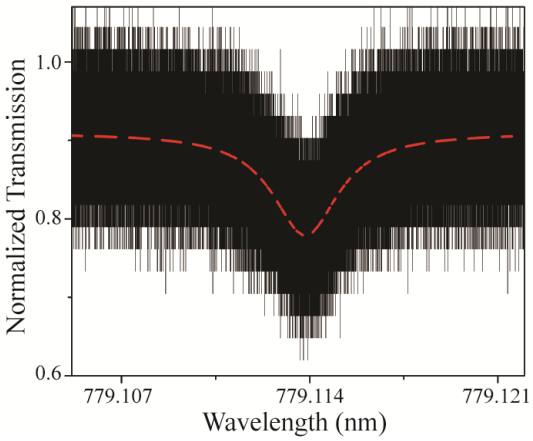

Fig. 3. A representative transmission spectra fit to a Lorentzian (dashed red line). The linewidth is 0.00298nm, yielding a loaded Q of 2.61×10^5.

4.2 Temperature sensing

As can be observed in Fig. 4(a), the resonant wavelength increases in direct response to each 0.5°C temperature increase. The background noise shown in the inset is determined by evaluating 240 seconds of the signal (N > 1600 pts). As such, it includes all sources of noise in the system, including taper jitter. The three sigma (3σ) value is similar to the mean loaded cavity linewidth (4.65 pm vs 6.2 pm). However, after a bandpass filter has been applied to remove the points with more than a 5% intensity variation, the 3σ noise level is reduced to 0.7pm. This improvement is readily apparent in the pair of noise histograms in Fig. 4(a), inset.

Throughout these measurements, the loaded cavity Q was fairly constant (Fig. 4(b)). As mentioned, the coupling was not actively changed during the measurements. Therefore, the overall decreasing trend could be attributed to a decrease in coupling efficiency or an increase in coupling loss. This decrease results in an increase in the extrinsic loss ($Q_{coupling}$), which will decrease the loaded Q. However, this change does not affect the underlying device's intrinsic Q. Additionally, the background noise level does not change substantially between the initial and the final measurements, and the reported noise values are at an intermediate temperature setting.

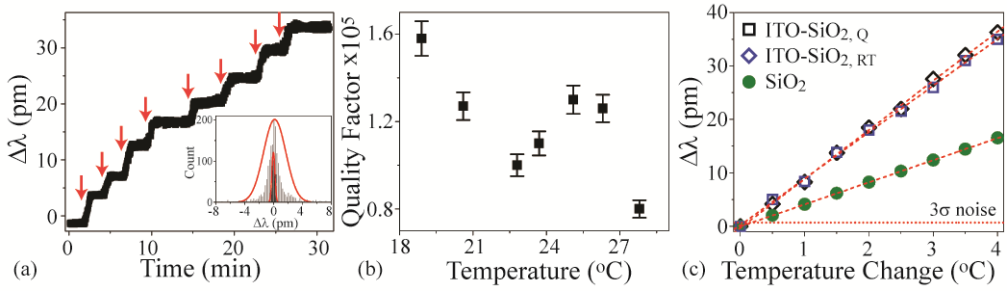

Fig. 4. a) Temperature sensing in real-time with noise. Inset: Histograms of the noise distributions with (gray) and without (black) the taper jitter filter. The results are fit to a Gaussian. b) The loaded cavity Q evolution throughout the measurement. c) The results from both measurement approaches are plotted for direct comparison. Additionally, the shift from a bare silica toroid and the baseline noise level are included.

The sensor response can be more explicitly evaluated if the wavelength shift versus temperature increment is plotted. In this sense, Fig. 4(c) shows the results from both measurement methods: 1) wavelength tracking in real-time (ITO-$SiO_{2,\ RT}$) and 2) measuring

#224193 - $15.00 USD Received 1 Oct 2014; revised 20 Nov 2014; accepted 25 Nov 2014; published 26 Jan 2015

the spectra at discrete time points (ITO-$SiO_{2,Q}$). Most importantly, the results are clearly self-consistent. For comparison, we have also plotted the baseline noise level and the theoretically predicted shift from a pure SiO_2 device. It is important to note that the shift from an environmental temperature change is independent of Q, unlike a shift induced by the opto-thermal effect which gives rise to linewidth broadening [26, 27]. Therefore, the fact that the SiO_2 toroid has a higher Q does not play a role in the magnitude of the sensor response.

The change in resonant wavelength in the ITO-SiO_2 hybrid cavity is significantly larger than the SiO_2 device. This improvement in device performance is directly related to the increase in the effective thermo-optic coefficient of the cavity, which now has varied from $1.2x10^{-5}$ °C to $1.712x10^{-5}$ °C due to the presence of the ITO thin-film. This increase is surprising given the relative distribution of the optical field in the SiO_2 and the ITO and indicates that the ITO has a very large, positive thermo-optic response.

By combining the simulation and spectroscopic ellipsometry results with Eqs. (4) and 5, the thermo-optic coefficient of ITO is calculated to be $2.229x10^{-4}$. This value is approximately 18 times larger than the thermo-optic coefficient of silica ($1.2x10^{-5}$ °C). Unfortunately, there is minimal previous work studying the dn/dT of ITO for comparison. However, in previous studies of TiO_2 films on SiO_2, a significant dependence of the dn/dT on the deposition method was observed, with over an order of magnitude variation [28]. Therefore, given these previous studies on TiO_2, additional investigation into the optimization of the deposition method to maximize the dn/dT is warranted.

5. Conclusion

In conclusion, we have fabricated and characterized an ITO-coated silica toroidal microcavity temperature sensor. After optimizing the ITO coating method to reduce defects in the ITO film, material limited quality factors ($>10^5$) are achieved. The narrow cavity linewidth in combination with a taper jitter reduction algorithm reduces the baseline noise, improving the overall signal-to-noise of the sensor system. Additionally, the dn/dT of ITO is nearly 20-fold larger than the underlying silica device. As a result of this increase, the thermal response of the hybrid ITO-SiO_2 sensor is more than doubled. Given the high thermal and chemical stability of both silica and ITO, this hybrid device could be used in many applications requiring high precision temperature detection, such as temperature monitoring in harsh environments. Additionally, the general device architecture is translatable to other refractometric-based sensor platforms, including microrings, waveguides and lasers.

Acknowledgments

This work has been supported by institutions both in Spain and in the USA. A Pre-doctoral Research Grant of the Public University of Navarra and the Spanish Ministry of Economy and Competitiveness FEDER TEC2013-43679-R project from Spain. Also, the National Institute of Health through the Director's New Innovator Award Program [1DP2OD007391-01] from the United States of America.